Ocean Sci. Discuss., 12, 1537–1566, 2015
www.ocean-sci-discuss.net/12/1537/2015/
doi:10.5194/osd-12-1537-2015

Ocean Science
Discussions
Open Access

Bio-optical characterization and light availability parametrization in two glacial melt water influenced estuary systems (West-Greenland)

L. Holinde and O. Zielinski

Institute for Chemistry and Biology of the Marine Environment, University of Oldenburg, Carl-von-Ossietzky-Str. 9–11, 26129 Oldenburg, Germany

Received: 04 June 2015 – Accepted: 22 June 2015 – Published: 21 July 2015

Correspondence to: L. Holinde (lars.holinde@uni-oldenburg.de)

Published by Copernicus Publications on behalf of the European Geosciences Union.

Abstract

Estuary systems are well-defined semi-enclosed systems which are strongly influenced by their terrestrial and marine boundaries. In this paper we investigate the bio-optical conditions in the water column of two neighboring estuary systems, Uummannaq Fjord and Vaigat–Disko Bay, in West Greenland. Though close to each other, the systems differ by their hydrographic structure influencing the bio-optical conditions and subsequently the biological activities. Both systems show high inorganic suspended particulate matter (SPMi) concentrations near freshwater respective melt water influxes (max. of 15.28 $mg\,L^{-1}$ at the surface) and low colored dissolved organic matter (aCDOM@350 nm, $< 1.50\,m^{-1}$) abundance throughout the estuaries. Chlorophyll as an indicator of phytoplankton was solely high in the Vaigat (max. of 11.44 $\mu g\,L^{-1}$) representing the outflow arm of the Disko Bay. Light penetration depth as indicated by the 1 % depth of Photosynthetically Available Radiation (PAR) was dominated by chlorophyll and SPMi alike and reached from 12.2 to 41.2 m. Based on these characteristics an effective two component parameterization for the diffuse attenuation coefficient k_{PAR} was developed enabling to model light penetration depth as a relevant factor for bio-optical studies in Arctic environments under glacial melt water influence.

1 Introduction

Greenland's estuary systems are strongly influenced by their ocean and land boundaries. On the land side this includes influence by glacier activities and fresh water influx from melt water or river runoff. The ocean side is influenced by sea and coastal waters whose exchange can be restricted by a shallow sill.

Global change has a huge influence on these estuary systems due to melting and runoff of glaciers. The Disko Bay (West Greenland), which is fed by the Jakobshavn Isfjord, is especially subject to bio-optical and oceanographic changes (Hansen et al., 2012; Garaba and Zielinski, 2013). During an expedition with R/V *Maria S. Merian* in

OSD
12, 1537–1566, 2015

July/August 2012 (MSM 21/3) optical, physical and biological properties were acquired in several fjords of West Greenland and Iceland (Cembella et al., 2013) focusing on phytoplankton species distribution and abundance as an indicator of potential Harmful Algae Bloom (HAB) formation in Arctic waters. The expedition coincided with an increase of the Jakobshavn Isbræglacier as reported by Joughin et al. (2014) and an extreme melt of the overall Greenland ice sheet in 2012 (Nghiem et al., 2012).

Optical properties of these coastal water bodies are reported to be influenced by small particles mainly transported by river runoff and melt water. Lund-Hansen et al. (2010) analyzed the optical properties in the Kangerlussuaq Fjord, West Greenland, highlighting especially the relevance of the very fine particle fraction (2–6 µm) for the underwater light field. Light availability is a major factor for phytoplankton growth (Bannister, 1974; Vahtera et al., 2014) including bloom initiation and development. The objective of this paper is to compare and classify the bio-optical characteristics of two estuary systems on the coast of West Greenland that are located in the same geographical area but governed by a different hydrography and geography. To achieve this goal, we will focus (i) on the abundance and statistics of chlorophyll *a* (Chl *a*), inorganic suspended particulate matter (SPMi) and colored dissolved organic matter (CDOM) and (ii) the resulting light penetration depth of the Photosynthetically Available Radiation (PAR) from field observations. Combining the both, we will (iii) derive an effective two component model for PAR in the water column from Chl *a* and SPMi observations, thus enabling an assessment of light availability in both systems in a novel integrated physical-bio-optical representation.

2 Research area and methods

2.1 Research area

Expedition MSM 21/3 started at Nuuk (Greenland) on 25 July 2012 and ended 10 August 2012 in Reykjavik (Iceland). Data shown in this paper are from Uummannaq Fjord,

OSD
12, 1537–1566, 2015

Vaigat and Disko Bay (Fig. 1). The Uummannaq Fjord is situated on the west coast of Greenland with its mouth at 71° N and 55° W. The main orientation of the fjord is south-east to north-west. The fjord has several inlets and tributary fjords. One of these tributary fjords is the Perlerfiup Kangerlua Fjord. The fjord flows into the Uummannaq Fjord at 71.05° N and 52° W near the Alfred-Wegener-Halvø (station 506) and is terminated to the east by the Perlerfiup Sermia Glacier (station 507). The fjord system is strongly influenced by melt water runoff from inland glaciers, opens to the west towards the oceanic waters of the Baffin Bay and is influenced by the West Greenland current traveling along the coast from south to north (Cuny et al., 2005; Munchow et al., 2006).

The Vaigat–Disko Bay area is located south of the Uummannaq Fjord. In contrast, it is an open system where the water enters on the south-western end of the Disko Bay and flows out mainly through the Vaigat (station 510–513) or in a westward counter current south of Disko Island. In addition, the Vaigat is strongly influenced by melt water runoff. A second important feature is the Jakobshavn Isfjord near station 514 which is fed by three glaciers and transports huge amounts of icebergs into the Disko Bay (Joughin et al., 2014).

2.2 Methods

2.2.1 In-situ measurements

Measurements were performed at seven stations in the Uummannaq Fjord (Fig. 1b, 503–509) and eight stations in the Vaigat–Disko-Bay area (Fig. 1b, 510–517) with different instruments (Table 1). At each measurement station a cast with a Conductivity-Temperature-Depth probe (CTD, SBE 911+, Sea-Bird Electronics Inc., USA) was performed. The temperature and salinity profiles were used to determine the hydrographic structure of the water body. Attached to this probe were a water sampler with 24 free flow bottles and a combined turbidity-fluorometer sensor (ECO-AFL/FL, WET Labs, USA, 470/695 nm fluorescence) for bio-optical measurements (Moore et al., 2009). Water samples were taken during the up cast at 3, 8, 15 m, deep chlorophyll max and

OSD
12, 1537–1566, 2015

from greater depth depending on the measurements from the downcast. These water samples were used to quantify total and inorganic suspended particulate material (SPM) and chlorophyll *a* (Chl *a*) concentrations. In addition, filtered water samples were used for absorption measurements (AquaLog, Horiba Ltd., Japan).

Depending on daylight and weather conditions measurements of the underwater light field and further bio-optical parameters were conducted utilizing a HyperPro II Profiler (Satlantic Inc., Canada). At these stations three casts were performed lowering (free falling) the profiler until the downwelling irradiance values were in the same order of magnitude as the dark current. The profiler contains different sensors from which we used a sensor measuring downward irradiance (E_d, HyperOCR Radiometer, Satlantic Inc., Canada) as well as an integrated CTD for depth measurements. In addition, an ECO Puck (WET Labs, USA) sensor was installed in the profiler configured to measure backscatter intensities at 700 nm. At an elevated, non-shaded location a downward irradiance (E_s, HyperOCR Radiometer, Satlantic Inc., Canada) reference sensor was mounted. Profiler data processing and calculation of desired parameters (backscatter and PAR) was performed applying ProSoft 7.7.16 (Satlantic Inc., Canada). ProSoft was setup for 0.2 m depth bins and 5 nm wavelength bins. After the processing with ProSoft, the depth grid was changed to 0.25 m bins and the mean of all profiles at each station was calculated to get the average light field data for the later processing.

2.2.2 Laboratory measurements

Table 2 provides an overview of the laboratory methods used and their probable errors. Water taken during the CTD casts was filtered to obtain the SPM concentrations using glass fiber filters (Whatman GF/F) with a mean pore size of 0.7 µm. Before the expedition filters had been heated at 500 °C for 5 h to remove biological remains and washed with ultrapure water to remove further remains in the filter. After drying at 60 °C for at least 6 h, the filters were weighted (Kern 770–60, KERN and SOHN GmbH, Germany) and packed as individuals. During the cruise, a defined water volume between 1 and 8 L, depending on filter clogging, was filtered. After filtration the filters were frozen at

OSD
12, 1537–1566, 2015

−20 °C. Following the cruise the filters were dried at 60 °C for at least 6 h and weighted deriving the total SPM content. Afterwards, filters were heated at 500 °C for 5 h and weighted again to derive the inorganic SPM concentration.

For concentrations of Chl *a* water volumes between 100 and 500 mL were filtered under low vacuum through Whatman GF/F filters with nominal pore size of 0.7 µm and directly frozen at −80 °C. After the cruise, pigment extraction was performed in a 90 % acetone solution, overnight at 4 °C. The extract was centrifuged for 10 min at 3020 × *g*. Fluorescence of the supernatant was measured with a pre–calibrated TD–700 laboratory fluorometer (Turner Designs, Sunnyvale, CA, USA). Computation of Chl *a* concentration (µg L^{-1}) was done according to EPA Method 446.0 protocol (Arar, 1997).

For CDOM analysis, water samples were filtered with a 0.2 µm filter (Membrane filter, Whatman) into a cuvette with a path length of 1 cm which was rinsed with purified water (MilliQ) and two times rinsed with sample water before. The sample was than measured in comparison to a sample of purified water (MilliQ). Measurement chamber was kept at 20 °C utilizing a stabilized thermobath for consistent measurements. Spectroflurometer (AquaLog, Horiba Ltd., Japan) was configured for measurements and calculation of CDOM absorption at different wavelengths (photometer option of the AquaLog).

2.2.3 Comparison between in-situ and laboratory data

To correlate in-situ Chl *a* fluorescence and laboratory Chl *a* concentrations Eq. (1) was chosen since its exponential slope reflects faster increasing concentrations compared to the resulting fluorescence signals Duyens (1956):

$$\text{Chl } a_{\text{fluo}} = a \times \exp(-b \times \text{Chl } a_{\text{con}}) + a. \quad (1)$$

In addition, SPMi concentrations were calculated from turbidity readings following Gohin (2011) which takes into account the measured Chl concentrations as a proxy for

OSD
12, 1537–1566, 2015

organic SPM:

$$\text{Turbidity} = c \times \left(\text{SPMi} + 0.234 \times \text{Chl}\, a_{\text{con}}^{0.57}\right). \quad (2)$$

After solving both equations, the equations were reversed to derive Chl *a* and SPMi concentrations from measured bio-optical properties.

2.2.4 Calculation of PAR

As mentioned above, light profile availability was limited to daylight conditions. Therefore we additionally adopted a simplified PAR model (compare Zielinski et al., 2002 for the impact of different PAR representations). According to Paulson and Simpson (1977) and Buiteveld (1995) it is possible to derive PAR at the depth z with the following simple relation

$$\text{PAR}(z) = \text{PAR}(0) \times \exp(-k_{\text{PAR}} \times z), \quad (3)$$

with (according to Gohin et al., 2005; Nelson and Smith, 1991):

$$k_{\text{PAR}} = d + e \times \text{SPMi} + f \times \left(\text{Chl}\, a_{\text{con}}^{g}\right). \quad (4)$$

In Eq. (4) the coefficient d represents the combined influence of pure sea water and CDOM absorption on the diffuse absorption coefficient k_{PAR}. Coefficients e and f represent the combined specific absorption and scattering factor for SPMi and Chl *a* and g the non-linearity of Chl *a* abundance and its absorption e.g. by the packaging effect. Whereas in most simple models k_{PAR} is considered constant for the water column, in our case the values for inorganic SPM (SPMi) and Chl *a* are changing between low concentrations and layers of significantly higher concentrations. Therefore we modified Eq. (3) in the following iterative way:

$$\text{PAR}(z(i)) = \text{PAR}(z(i-1)) \times \exp(-k_{\text{PAR}} \times (z(i) - z(i-1))). \quad (5)$$

The 1 % depth PAR was calculated by solving Eq. (5) while assuming 100 % at the top of the water column and then searching for the depth nearest to 1 %.

OSD
12, 1537–1566, 2015

3 Results

3.1 Data overview

Data obtained during expedition MSM 21/3 is available at World Ocean Data Center PANGAEA (Zielinski et al., 2013a, b, c, d). Figures 2 and 3 show the hydrographic and bio-optical conditions in both estuary systems. The data from the Uummannaq Fjord is displayed starting at the Perlerfiup Sermia Glacier (507) and ending at the ocean boundary (503). In the Vaigat–Disko Bay the data is displayed following the station numbering. In the Uummannaq Fjord a top layer of warm water was observed followed by a layer of colder water between 25 and 125 m below which the water is getting warmer again. An exception is station 507 where the difference between the warm and cold layer is smaller than at other stations in the Fjord. The salinity in the Uummannaq Fjord shows increasing values from the top towards the bottom with the lowest values at top of station 506. Some stations in Vaigat–Disko Bay show a similar top layer of warm water compared to the Uummannaq Fjord stations. In the Vaigat the temperature of this layer is colder than in the fjord. At stations 515 to 517 the temperatures are similar compared to the fjord data. Station 514 (Jakobshavn Isfjord) shows a very cold top layer before the temperature first increases and then decreases again. The other stations show a similar cold layer below the warm top layer before the temperature rises again. Nearly all station show a top layer of lower salinity values with exceptions near the Jakobshavn Isfjord and south of Disko Island.

Figure 3 shows Chl *a* fluorescence (top), turbidity (middle) and PAR (bottom). For the Uummannaq Fjord the fluorescence values are very low. Only a small layer near the ocean boundary shows higher values (3 RU). Disko Bay shows similar low values. The highest measurements were obtained during the inner stations in the Vaigat with the maximum at the top of the water column at station 512 (up to 8 RU). Turbidity shows the highest values at stations with fresh water runoff or glacier influence. At these stations the values rise up to 2 NTU. The PAR measurements show some gaps in the data due to stations without profiler measurements. The PAR penetration depth changes strongly

OSD
12, 1537–1566, 2015

between 17.25 and 38.75 m in the Uummannaq Fjord and between 11.5 and 41.5 m in the Vaigat–Disko Bay for the 1 % PAR depth. These values are strongly related with the fluorescence and turbidity measurements at the respective stations.

Table 3 summarizes range, mean and standard deviation in a separated table for both regions of interest. While temperature, aCDOM@350 nm and PAR 1 % depth show no significant differences, SPMi is more abundant in the Uummannaq Fjord and Chlorophyll maximum ranges are higher in the Vaigat. Low salinity ranges in the Disko Bay originate from the Jakobshavn Isbræ melt water influx.

Figure 4 illustrates the laboratory data as comparison of different depth levels. The Chl *a* concentrations in Fig. 4a and b show the highest concentrations in the Vaigat (510–513) similar to the fluorescence measurements from the CTD. Figure 4c and d show the greatest SPM concentrations at stations 503 and 504 this is in contrast to the turbidity measurements from the CTD. Similar differences can be observed by comparing laboratory and in-situ data for station 513 and 517. The CDOM absorption (Fig. 4e and f) changes between each station with the highest values at 50 m depth near the Jakobshavn Isfjord. Other high values can be generally observed at stations which are closer towards the open ocean (503, 509, and 517).

3.2 Comparison of in-situ and sampled data, and modeling of PAR

Based on the full dataset a multi-parameter fit (MATLAB R2013b) was performed for the exponential correlation of Eq. (1) between Chl *a* concentration and fluorescence from the same depth leading towards:

$$\mathrm{Chl}a_{\mathrm{fluo}} = -9.2 \times \exp(-0.08 \times \mathrm{Chl}\ a_{\mathrm{con}}) + 9.2. \quad (6)$$

Figure 5 shows a scatter plot of Chl *a* concentration and fluorescence as well as the result of Eq. (6) ($R^2 = 0.70$). The error of the unknown coefficients is estimated to be smaller than 17 %.

Parameterization of Eq. (2) was derived from laboratory SPMi and Chl *a* concentrations as well as in-situ turbidity data for depth were SPMi measurements were available

OSD
12, 1537–1566, 2015

again by a multi-parameter optimization:

$$\text{Turbidity} = 0.4968 \times \left(\text{SPMi} + 0.234 \times \left(\text{Chl}\, a_{\text{con}}^{0.57}\right)\right). \quad (7)$$

The scatter plot between the sum of SPMi and the Chl *a* concentration and the turbidity together with the graph from Eq. (7) ($R^2 = 0.70$) are shown in Fig. 6a. The graph shows some high SPMi data from stations 503–505 (red dots Fig. 6a) with corresponding low turbidity data compared to the correlation for the other measurements. A comparison between backscatter and turbidity signals (Fig. 6b) shows a good correspondence ($R^2 = 0.82$) for all data from the two optical in-situ methods. This suggests that some SPMi measurements are too high. Therefore measurements were excluded from the regression. The error of the Eq. (7) due to measurement accuracy and methods is below 26 %.

Equation (4) was solved using Curve Fitting Tool from MATLAB with default options and laboratory data and corresponding available k_{PAR} measurements from the profiler from the same depth resulting in with an error smaller than 30 %:

$$k_{\text{PAR}} = 0.07848 + 0.0573 \times \text{SPMi} + 0.04228 \times \left(\text{Chl}\, a_{\text{con}}^{0.8226}\right) \quad (R^2 = 0.41). \quad (8)$$

Utilizing Eq. (8) k_{PAR} was calculated for every depth z and subsequently used in Eq. (5) for calculation of available light in % at each depth. From these results the 1 % PAR depth was calculated as the depth with the nearest value towards 1 %. Figure 7 shows a comparison between the measured and modeled 1 % depth ($R^2 = 0.92$). The differences between the measured and modeled data range from 0.7 % (504) to 15.1 % (514).

3.3 Integrated bio-optical representation

The results from in-situ measurements and the correlation equations (6) and (7) were integrated into a graphical representation of the bio-optical factors together with the

OSD
12, 1537–1566, 2015

measured and modeled 1 % depth of PAR (Eqs. 5 and 8). The concentrations of Chl *a* and SPMi were integrated between the top of the water column and the modeled 1 % PAR depth. The integrated values are presented by the size of the triangles for Chl *a* and squares for SPMi at the depth of the Chl *a* maximum (DCM, deep chlorophyll max) or SPMi maximum (DSM, deep SPMi max).

Highest integrated concentrations of Chl were observed in the Vaigat (Fig. 9, stations 510–513) with values between 121.9 and 452.8 mg m^{-2}. The integrated concentrations at the other stations ranged from 14.3 to 174.2 mg m^{-2}. Depth of the DCM was between 2 and 12.5 m in the Vaigat and 17 and 35.5 m in Disko Bay. In the Uummannaq Fjord the DCM was found between 9.5 and 28.5 m. With exception of station 510, Chl maximum was always above the 1 % penetration depth of PAR for the stations where light measurements were available. At station 510 the DCM depth is equal to the 1 % PAR depth.

Integrated SPMi concentrations were highest in front of the Perlerfiup Sermia Glacier (507) with 200.6 g m^{-2} and at the first station in the Vaigat (510, located near a runoff) with 179.3 g m^{-2}. At station 506 and 507 the SPMi was mainly located near the water surface (Fig. 3c) resulting in a strong turquoise coloring of the water as observed from above. The overall SPMi concentration is decreasing from semi enclosed stations to stations in more open areas. Lowest concentrations were measured in areas towards the open sea of both Uummannaq Fjord and Disko Bay. The depth of the SPMi maximum varied between 1.5 and 37.5 m.

The 1 % depth of PAR varied strongly between stations of high Chl and/or SPMi concentrations and stations where both concentrations were low. This results in depth ratings of 11.5 m in the Vaigat and 17.25 m in front of the Perlerfiup Sermia Glacier while in the open areas of the Uummannaq Fjord and Disko Bay the 1 % PAR depth increased to 38.75 and 41.5 m. The modeled 1 % PAR depth follows the general trend of the measured 1 % PAR depth.

OSD
12, 1537–1566, 2015

4 Discussion

4.1 Comparison of in-situ methods and sampled data

Chlorophyll distribution could be successfully derived from in-situ fluorescence profiles calibrated by laboratory analysis ($R^2 = 0.70$) based on a parameterization of Duyens (1956).

SPMi distribution was derived with Eq. (7) ($R^2 = 0.69$) from Gohin (2011) from laboratory data. Stations 503–505 were excluded from the linear model due to very high SPM concentrations compared to low turbidity measurements probably originating from too long retention times before sampling from the bottles during these initial stations of the cruise. Due to this time lag sediment particles in the water sampler accumulated at the bottom before the water was sampled. The significant correlation between the turbidity and backscatter values indicates the coherence quality of the in-situ optical methods underlining this assumption.

PAR profiles were derived based on an adopted model of Buiteveld (1995) with local parameterization of k_{PAR} following Gohin et al. (2005). Comparison with measured PAR profiles respectively their calculated 1 % depth of PAR show a good correlation ($R^2 = 0.92$) with a slight underestimation of the penetration depth for some stations. The model is appropriate for rapid estimates of light availability within these melt water influenced Arctic estuaries based on water sample analysis and common bio-optical sensors within CTD profiles.

4.2 Comparison Uummannaq Fjord and Vaigat–Disko Bay

Although the two systems, Uummannaq and Vaigat–Disko Bay, are in same area of West-Greenland and both are estuary systems fed by the same inland glacier as well as opening up to the same ocean end member (the Baffin Bay), there are substantial differences in their bio-optical conditions. Based on our observations, the Vaigat has the highest Chl *a* concentrations ($> 10\,\mu g\,L^{-1}$) while Uummannaq Fjord and Disko Bay

OSD
12, 1537–1566, 2015

show smaller Chl concentrations. Similar results for the Vaigat were obtained in August 1993 by Jensen et al. (1999). Satellite imagery of Chl *a* concentrations for July/August 2012 (http://oceancolor.gsfc.nasa.gov/cms/, access 29 April 2015) show similar values for the research area. This indicates that most of the primary production occurs in the Vaigat during this time of year while Uummannaq Fjord and Disko Bay have only smaller influence on biomass production. A potential reason for the higher concentrations in the Vaigat can be the favorable current system in the Disko Bay as well as fresh water runoff from the glaciers. A model for the system was described by Ribergaard et al. (2004) showing that the water enters the bay at the south west corner. From there it flows through the bay and outwards through the Vaigat. In contrary Heide-Jørgensen et al. (2007) report higher Chl *a* concentrations for April to June for the years 2001 till 2004 in Disko Bay then in Vaigat derived from satellite observations. As their data was acquired earlier in the year this suggest an earlier algae bloom in Disko Bay following the winter ice cover melt which depletes most nutrients for later algae growth.

In the Uummannaq Fjord most of the surface water flows from the glaciers towards the open ocean. This water is rich on mineral particles near the glacier but only contains very small amounts of phytoplankton. The high concentration of mineral particles originates from melting glacier ice and runoff into the fjord. This leads to a horizontal SPM gradient in the fjord and to vertical distributions in the water column especially where low density water floats near the surface. It can be speculated that the strong melting reported for 2012 was also leading to increased inorganic SPM influxes; however this needs to be validated from either multiyear observations or sediment sampling. Lund-Hansen et al. (2010) sampled in the Kangerlussuaq Fjord at the beginning of August 2007. Their results show similar low Chl *a* concentrations as in the Uummannaq Fjord which is of comparable general geography as the Kangerlussuaq Fjord. The SPMi concentrations are slightly higher for most stations in the Kangerlussuaq Fjord.

Mean aCDOM values measured in both estuaries show a similar range (Table 3). Lund-Hansen et al. (2010) published CDOM absorption values at 440 nm for the Kangerlussuaq Fjord. These values range from 0.046 to 0.36 m^{-1} with the higher val-

OSD
12, 1537–1566, 2015

ues near melt water outlets. Converting the aCDOM results from Table 3 to 440 nm leads to similar values with mean values of 0.07 m^{-1} (Uummannaq) and 0.11 m^{-1} (Vaigat–Disko Bay) and maxima up to 0.48 and 0.61 m^{-1}. Lower variability was observed towards the Perlerfiup Sermia Glacier in the Uummannaq Fjord (Fig. 4e) compared to data from the outer fjord and Vaigat–Disko Bay (Fig. 4f) indicating influence from different sources in these areas.

Temperature and salinity data showed a top layer of warmer and less saline water. This is due to melt water influence and solar heating at the air-water surface. The melt water influence is also indicated by the higher SPMi concentrations at the water surface at some stations (e.g. 506 and 512, Fig. 3). Similar water structures were mentioned by Farmer and Freeland (1983) describing the general hydrographic structure of fjords.

4.3 Light penetration in an integrated bio-optical representation

High abundances of SPMi and Chl *a* have a huge influence on the light penetration depth as can be seen from the changes in the 1 % PAR depth in both estuary systems. In contrast, the CDOM absorption measurements only show lower values throughout this study suggesting that the influence of CDOM on the underwater light field is less relevant in these specific estuaries. Due to this, the absorption of CDOM was considered to be constant in the PAR model and combined with the pure seawater attenuation in Eq. (4). Based on this approach and the bio-optical conditions observed a parameterization of the diffuse attenuation coefficient k_{PAR} was specified (Eq. 8) and subsequently utilized to fill observational gaps due to lacking PAR profiles in unfavorable light conditions.

As expected the DCM is always above the 1 % PAR depth emphasizing the limiting role of light for photosynthetic growth. The DCM depth is also similar to or above the depth of the warm top layer detected in the estuary systems indicating a further limiting factor for photosynthetic growth. The integrating perspective taken in Figs. 8 and 9 presents and simplifies the bio-optical data to a comparative scale. The different resulting conditions, depending on the concentrations of Chl *a* and SPMi, and 1 %

OSD
12, 1537–1566, 2015

PAR depth of the two adjacent estuary systems are thus visualized enabling an easier assessment of the connection between the key variables for light availability in these estuary systems.

5 Conclusions

The results of this study are based on one research cruise in the two estuary systems. The time period of the cruise was characterized by an extreme melt of the Greenland ice cover and a resulting increase of melt water influx into the research areas. Although both systems are in the same general area Chl *a* was significantly more abundant in the Vaigat. SPMi concentrations were highest near freshwater influxes. CDOM absorption, examined here at 350 nm, showed only little differences between the two estuaries and the values were generally low.

Chl *a* and SPMi were identified as the main components influencing the underwater light field and the resulting 1 % PAR depth. For these components correlations were derived between optical in-situ measurements and laboratory measurements. Resulting from these correlations and the underwater PAR measurements a simple model was developed to fill observational gaps due to unfavorable light conditions during the research cruise.

Future investigations in this area will extend this concept of an integrated physical-bio-optical representation. Especially analysis and forecast of hyperspectral light availability will be of interest for bloom events but also the role of shallow areas and water mass influxes for bloom initiation.

Acknowledgements. We want to thank master and crew of the R/V *Maria S. Merian* as well as chief scientist Allan Cembella for their support during MSM21/3. Our gratitude is expressed to Daniela Meier, Daniela Voß and Rohan Henkel for their help during and after the expedition. We are grateful to Julia Busch, Mindy Richlen and Don Anderson for commenting parts of this manuscript.

OSD
12, 1537–1566, 2015

References

Amante, C. and Eakins, B. W.: ETOPO1 1 Arc-Minute Global Relief Model: Procedures, Data Sources and Analysis, doi:10.7289/V5C8276M, available at: http://www.ngdc.noaa.gov/mgg/global/global.html, (last access: 25 March 2015), 2009. 1558

Arar, E. J.: Method 446.0: In Vitro Determination of Chlorophylls a, b, c + c and Pheopigments in Marine And Freshwater Algae by Visible Spectrophotometry, Report, United States Environmental Protection Agency, Office of Research and Development, National Exposure Research Laboratory, Cincinatti, Ohio, USA, 1997. 1542

Bannister, T. T.: A general theory of steady state phytoplankton growth in a nutrient saturated mixed layer, Limnol. Oceanogr., 19, 13–30, doi:10.4319/lo.1974.19.1.0013, 1974. 1539

Buiteveld, H.: A model for calculation of diffuse light attenuation (PAR) and Secchi depth, Netherlands Journal of Aquatic Ecology, 29, 55–65, 1995. 1543, 1548

Cembella, A., Zielinski, O., Anderson, D., Graeve, M., Henkel, R., John, U., Kattner, G., Koch, B., Krock, B., Meier, D., Richlen, M., Tillmann, U., and Voß, D.: ARCHEMHAB: Interactions and feedback mechanisms between hydrography, geochemical signatures and microbial ecology, with a focus on HAB species diversity, biogeography and dynamics, Report, DFG-Senatskommission für Ozeanographie, Bremen, Germany, 2013. 1539

Cuny, J., Rhines, P. B., Schott, F., and Lazier, J.: Convection above the Labrador continental slope, J. Phys. Oceanogr., 35, 489–511, doi:10.1175/Jpo2700.1, 2005. 1540

Duyens, L. N. M.: The flattering of the absorption spectrum of suspensions, as compared to that of solutions, Biochim. Biophys. Acta, 19, 1–12, doi:10.1016/0006-3002(56)90380-8, 1956. 1542, 1548

Farmer, D. M. and Freeland, H. J.: The physical oceanography of Fjords, Prog. Oceanogr., 12, 147–219, doi:10.1016/0079-6611(83)90004-6, 1983. 1550

Garaba, S. P. and Zielinski, O.: Comparison of remote sensing reflectance from above-water and in-water measurements west of Greenland, Labrador Sea, Denmark Strait, and west of Iceland, Opt. Express, 21, 15938–15950, doi:10.1364/OE.21.015938, 2013. 1538

Gohin, F.: Annual cycles of chlorophyll-*a*, non-algal suspended particulate matter, and turbidity observed from space and in-situ in coastal waters, Ocean Sci., 7, 705–732, doi:10.5194/os-7-705-2011, 2011. 1542, 1548

Gohin, F., Loyer, S., Lunven, M., Labry, C., Froidefond, J. M., Delmas, D., Huret, M., and Herbland, A.: Satellite-derived parameters for biological modelling in coastal waters: illustration

OSD
12, 1537–1566, 2015

over the eastern continental shelf of the Bay of Biscay, Remote Sens. Environ., 95, 29–46, doi:10.1016/j.rse.2004.11.007, 2005. 1543, 1548
Hansen, M. O., Nielsen, T. G., Stedmon, C. A., and Munk, P.: Oceanographic regime shift during 1997 in Disko Bay, Western Greenland, Limnol. Oceanogr., 57, 634–644, doi:10.4319/lo.2012.57.2.0634, 2012. 1538
Heide-Jørgensen, M. P., Laidre, K. L., Logsdon, M. L., and Nielsen, T. G.: Springtime coupling between chlorophyll a, sea ice and sea surface temperature in Disko Bay, West Greenland, Prog. Oceanogr., 73, 79–95, doi:10.1016/j.pocean.2007.01.006, 2007. 1549
Jensen, H. M., Pedersen, L., Burmeister, A. D., and Hansen, B. W.: Pelagic primary production during summer along 65 to 72° N off West Greenland, Polar Biol., 21, 269–278, doi:10.1007/s003000050362, 1999. 1549
Joughin, I., Smith, B. E., Shean, D. E., and Floricioiu, D.: Brief Communication: Further summer speedup of Jakobshavn Isbræ, The Cryosphere, 8, 209–214, doi:10.5194/tc-8-209-2014, 2014. 1539, 1540
Lund-Hansen, L. C., Andersen, T. J., Nielsen, M. H., and Pejrup, M.: Suspended Matter, Chl-a, CDOM, grain sizes, and optical properties in the arctic Fjord-Type Estuary, Kangerlussuaq, West Greenland during summer, Estuar. Coast., 33, 1442–1451, doi:10.1007/s12237-010-9300-7, 2010. 1539, 1549
Moore, C., Barnard, A., Fietzek, P., Lewis, M. R., Sosik, H. M., White, S., and Zielinski, O.: Optical tools for ocean monitoring and research, Ocean Sci., 5, 661–684, doi:10.5194/os-5-661-2009, 2009. 1540
Munchow, A., Melling, H., and Falkner, K. K.: An observational estimate of volume and freshwater flux leaving the arctic ocean through nares strait, J. Phys. Oceanogr., 36, 2025–2041, doi:10.1175/Jpo2962.1, 2006. 1540
Nelson, D. M. and Smith, W. O.: Sverdrup revisited – critical depths, maximum chlorophyll levels, and the control of Southern-Ocean productivity by the irradiance-mixing regime, Limnol. Oceanogr., 36, 1650–1661, 1991. 1543
Nghiem, S. V., Hall, D. K., Mote, T. L., Tedesco, M., Albert, M. R., Keegan, K., Shuman, C. A., DiGirolamo, N. E., and Neumann, G.: The extreme melt across the Greenland ice sheet in 2012, Geophys. Res. Lett., 39, L20502, doi:10.1029/2012gl053611, 2012. 1539
Paulson, C. A. and Simpson, J. J.: Irradiance measurements in the upper ocean, J. Phys. Oceanogr., 7, 952–956, doi:10.1175/1520-0485(1977)007<0952:imituo>2.0.co;2, 1977. 1543

OSD
12, 1537–1566, 2015

Ribergaard, M. H., Pedersen, S. A., Ådlandsvik, B., and Kliem, N.: Modelling the ocean circulation on the West Greenland shelf with special emphasis on northern shrimp recruitment, Cont. Shelf Res., 24, 1505–1519, doi:10.1016/j.csr.2004.05.011, 2004. 1549

Vahtera, E., Crespo, B. G., McGillicuddy, D. J., Olli, K., and Anderson, D. M.: Alexandrium fundyense cyst viability and germling survival in light vs. dark at a constant low temperature, Deep-Sea Res. Pt. II, 103, 112–119, doi:10.1016/j.dsr2.2013.05.010, 2014. 1539

Zielinski, O., Llinas, O., Oschlies, A., and Reuter, R.: Underwater light field and its effect on a one-dimensional ecosystem model at station ESTOC, north of the Canary Islands, Deep-Sea Res. Pt. II, 49, 3529–3542, doi:10.1016/S0967-0645(02)00096-6, 2002. 1543

Zielinski, O., Voß, D., Meier, D., Henkel, R., Holinde, L., Garaba, S. P., and Cembella, A.: Physical oceanography during Maria S. Merian cruise MSM21/3 (ARCHEMHAB), PANGAEA – Data Publisher for Earth & Environmental Science, doi:10.1594/pangaea.819731, 2013a. 1544

Zielinski, O., Voß, D., Meier, D., Henkel, R., Holinde, L., Garaba, S. P., and Cembella, A.: Total suspended matter, particulate organic matter, and particulate inorganic matter during Maria S. Merian cruise MSM21/3 (ARCHEMHAB), PANGAEA – Data Publisher for Earth & Environmental Science, doi:10.1594/PANGAEA.810708, 2013b. 1544

Zielinski, O., Voß, D., Meier, D., Henkel, R., Holinde, L., Garaba, S. P., and Cembella, A.: Chlorophyll a during Maria S. Merian cruise MSM21/3 (ARCHEMHAB), PANGAEA – Data Publisher for Earth & Environmental Science, doi:10.1594/PANGAEA.810651, 2013c. 1544

Zielinski, O., Voß, D., Meier, D., Henkel, R., Holinde, L., Garaba, S. P., and Cembella, A.: Colored dissolved organic matter during Maria S. Merian cruise MSM21/3 (ARCHEMHAB), PANGAEA – Data Publisher for Earth & Environmental Science, doi:10.1594/PANGAEA.810861, 2013d. 1544

OSD
12, 1537–1566, 2015

Table 1. Accuracy of in-situ Instruments used in this paper.

Instrument	Parameter	Accuracy
CTD	Conductivity ($S\,m^{-1}$)	< 1 %
CTD	Temperature (°C)	< 1 %
CTD	Pressure (m)	< 1 %
ECO-AFL/FL	Fluorescence ($\mu g\,L^{-1}$)	< 1 %
ECO-AFL/FL	Turbidity (NTU)	< 1 %
Profiler	Pressure (dBar)	< 1 %
HyperOCR Radiometer	downwelling Irradiance (500 nm, 1024 ms integration time, $\mu W\,cm^{-2}\,nm^{-1}$)	< 5 %
HyperOCR Radiometer	reference Irradiance (500 nm, 1024 ms integration time, $\mu W\,cm^{-2}\,nm^{-1}$)	< 5 %
ECO Puck	Backscatter ($m^{-1}\,sr^{-1}$)	< 1 %

OSD
12, 1537–1566, 2015

Table 2. Uncertainties and accuracy for laboratory methods and instruments.

Parameter	Unit	Filter Volume Error	System	Accuracy	Method error	total error
SPM	$mg\,L^{-1}$	< 5 %	Kern 770–60	< 1 %	5 %	< 11 %
Chl *a*	$\mu g\,L^{-1}$	< 5 %	TD–700	< 1 %	10 %	< 16 %
CDOM	m^{-1}	–	Aqualog	< 5 %	5 %	< 10 %

OSD
12, 1537–1566, 2015

Table 3. Statistics of oceanographic and bio-optical data from the Uummannaq Fjord (left) and in Vaigat–Disko Bay (right). Each column is subdivided into minimum (min), maximum (max), mean and standard deviation (std). Rows show from top to bottom temperature in °C, salinity, Chl *a* in $\mu g\,L^{-1}$, suspended particulate matter in $mg\,L^{-1}$, CDOM absorption (aCDOM) at 350 nm in $1\,m^{-1}$ and 1 % depth of Photosynthetically Available Radiation (PAR) in m.

	Uummannaq Fjord				Vaigat–Disko Bay			
	min	max	mean	std	min	max	mean	std
Temperature (°C)	−1.55	9.78	1.96	1.35	0.53	10.20	2.26	1.06
practical Salinity	27.00	34.94	34.02	0.71	15.56	34.52	33.78	0.76
Chl *a* ($\mu g\,L^{-1}$)	0.1	2.7	0.8	0.6	0.1	11.4	3.0	3.7
SPMi ($mg\,L^{-1}$)	0.1	15.3	5.1	4.4	0.1	9.1	2.0	2.4
aCDOM@350 nm ($1\,m^{-1}$)	0.0	1.4	0.3	0.2	0.0	1.5	0.4	0.3
PAR 1 % (m)	17.3	38.8	29.0	9.0	11.5	41.5	33.9	12.8

OSD
12, 1537–1566, 2015

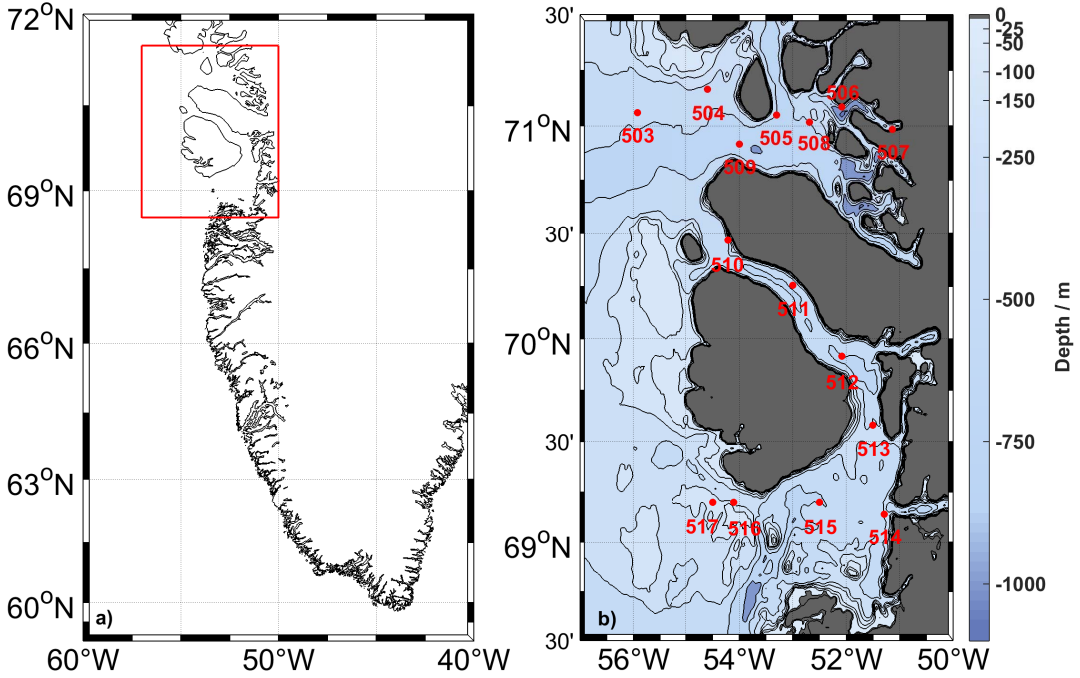

Figure 1. (a) Map of Greenland and parts of Baffin Bay, **(b)** study area: Uummannaq Fjord, Vaigat and Disko Bay (West Greenland) with stations (red dots) and under water topography (data from Amante and Eakins, 2009). The contour lines represent the indicated depth at the colorbar next to the map.

OSD
12, 1537–1566, 2015

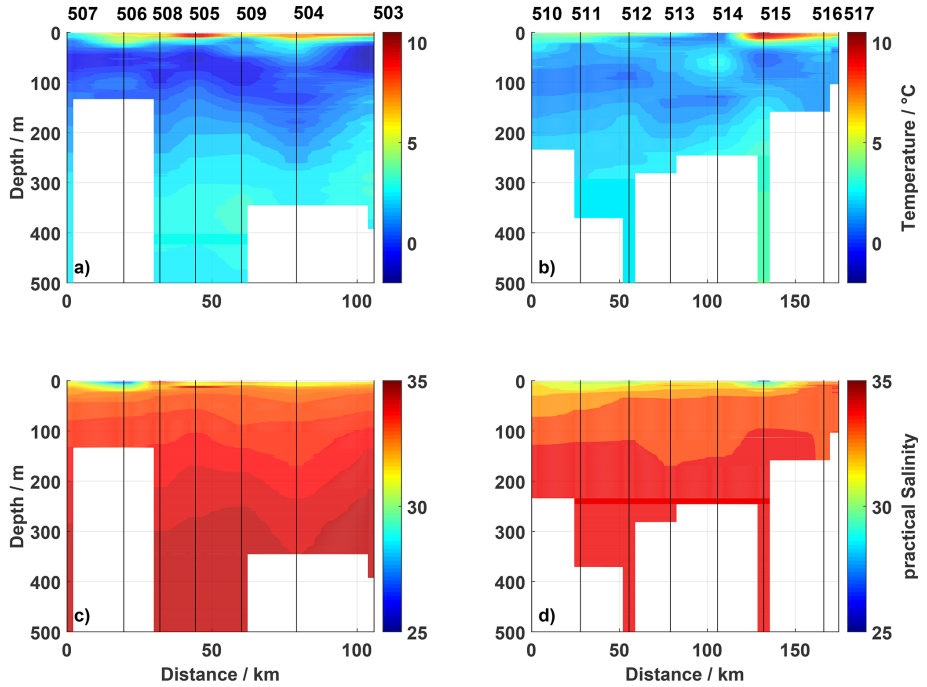

Figure 2. Hydrographic conditions in the Uummannaq Fjord (left, **a, c**) and in Vaigat–Disko Bay (right, **b, d**). At the top temperature and at the bottom salinity is shown.

OSD
12, 1537–1566, 2015

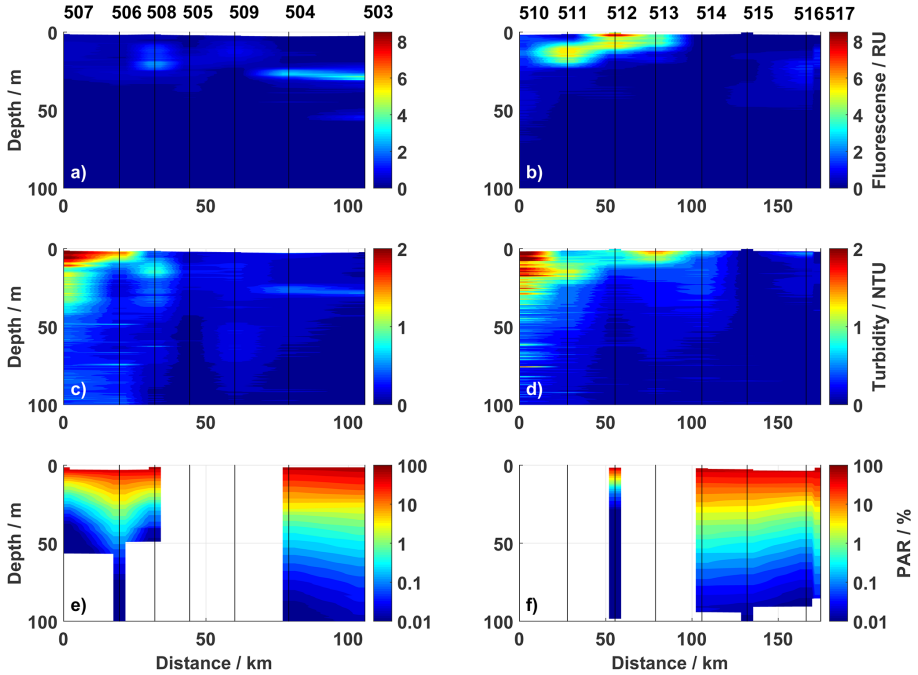

Figure 3. Bio-optical conditions in the Uummannaq Fjord (left, **a, c**, and **e**) and in Vaigat–Disko Bay (right, **b, d**, and **f**). At the top the Chl *a* fluorescence, in the middle turbidity and at the bottom PAR in % of surface PAR are shown.

OSD
12, 1537–1566, 2015

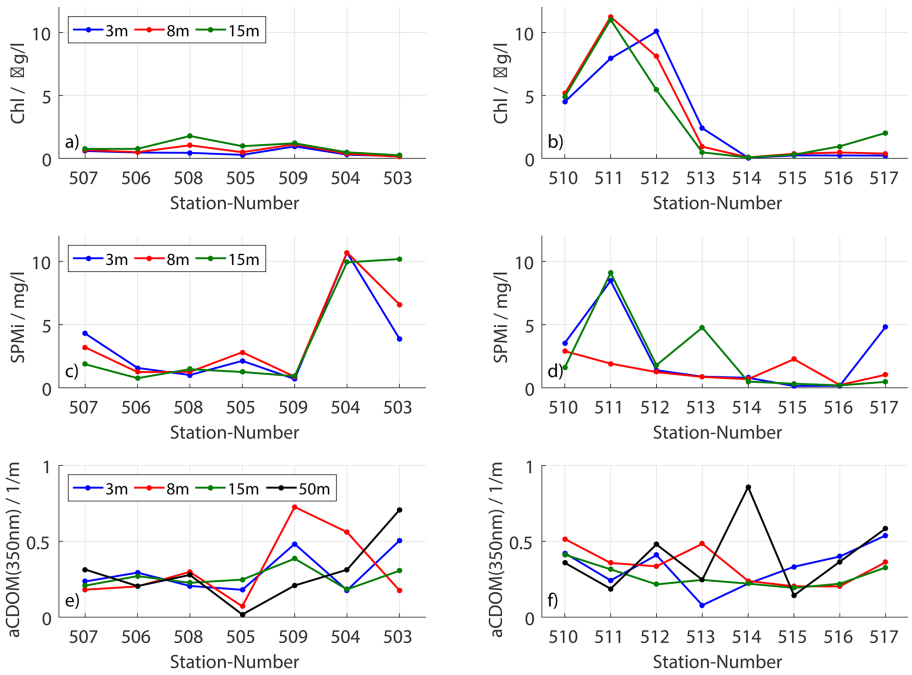

Figure 4. Comparison of laboratory Chl *a* concentrations at 3 m (blue), 8 m (red), 15 m (green) are presented in **(a)** (Uummannaq Fjord) and **(b)** (Vaigat–Disko Bay). Highest concentrations were observed in the Vaigat (510–513). Graphs **(c, d)** show laboratory SPMi concentrations at the same depth. CDOM(350 nm) absorption is displayed at in **(e, f)** at the depth mentioned before and in addition at 50 m.

OSD
12, 1537–1566, 2015

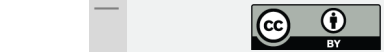

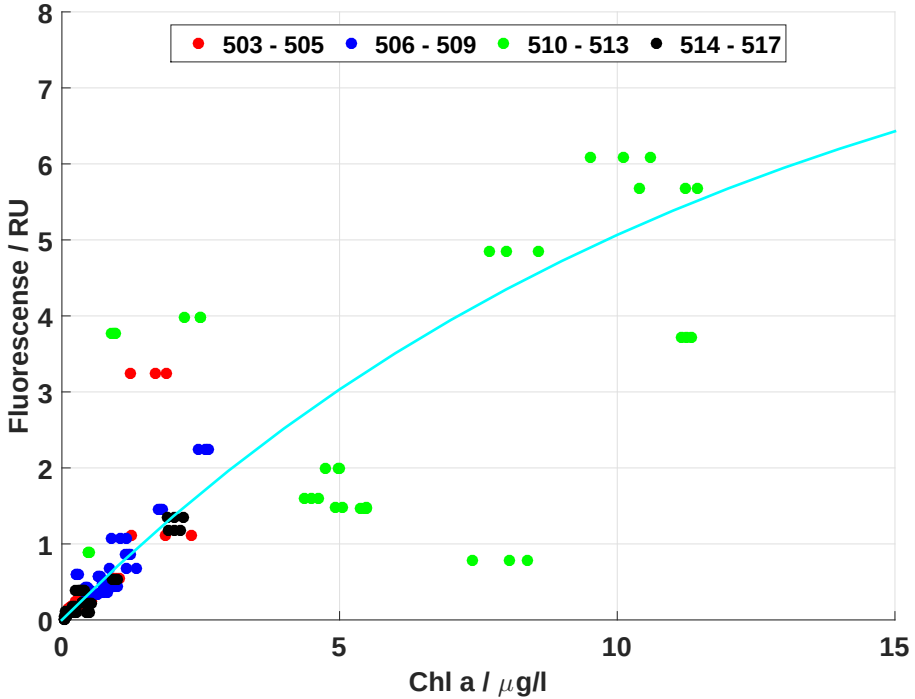

Figure 5. Comparison between Chl *a* concentrations and chlorophyll fluorescence for the CTD casts. The cyan line represents Eq. (6). Red and blue dots represent stations in the Uummannaq Fjord; green dots are stations in Vaigat and black dots are stations in Disko Bay.

OSD
12, 1537–1566, 2015

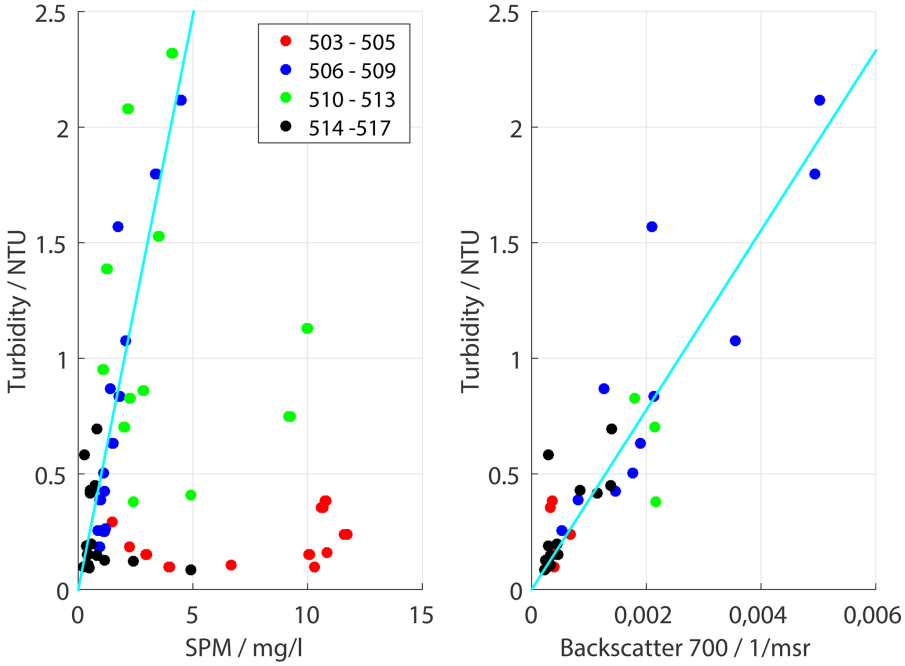

Figure 6. Left: comparison between SPM and turbidity measurements from the CTD casts. The cyan line represents Eq. (7). Right: comparison between backscatter signal at 700 nm from the profiler and turbidity data from the CTD as well as correlation between the two measurement systems (cyan line). Red and blue dots represent stations in the Uummannaq Fjord; green dots are stations in Vaigat and black dots are stations in Disko Bay.

OSD
12, 1537–1566, 2015

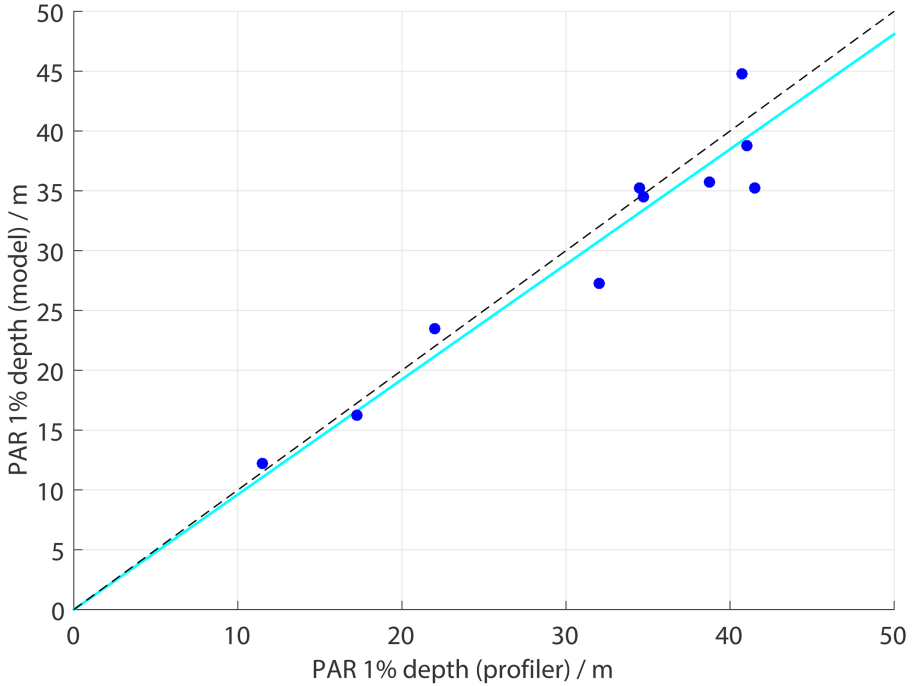

Figure 7. Comparison between measured and modeled 1 % PAR depth. The cyan line represents the best linear correlation between the two parameters (R^2 = 0.92) and the dashed black line the 1 : 1 correlation.

OSD
12, 1537–1566, 2015

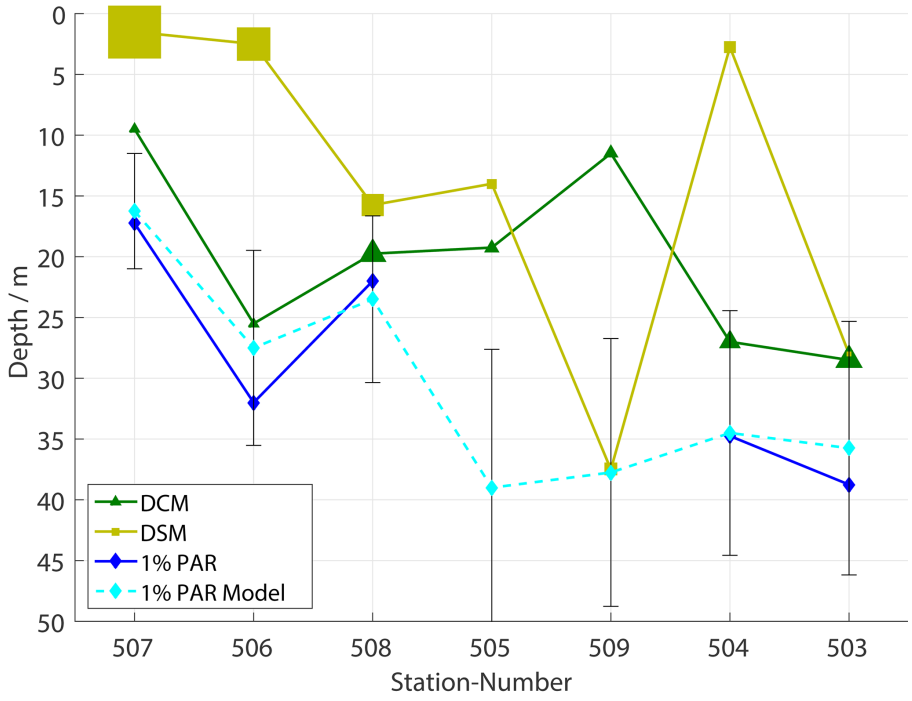

Figure 8. DCM (green, deep chlorophyll max) and DSM (ocher, deep SPMi max) at all stations in the Uummannaq Fjord from west to east. The size of the markers represents the integrated Chl *a* and SPMi concentrations from the top of the water column to the modeled 1 % depth. Measured 1 % PAR (blue) where available and modeled 1 % PAR as dashed line (cyan).

OSD
12, 1537–1566, 2015

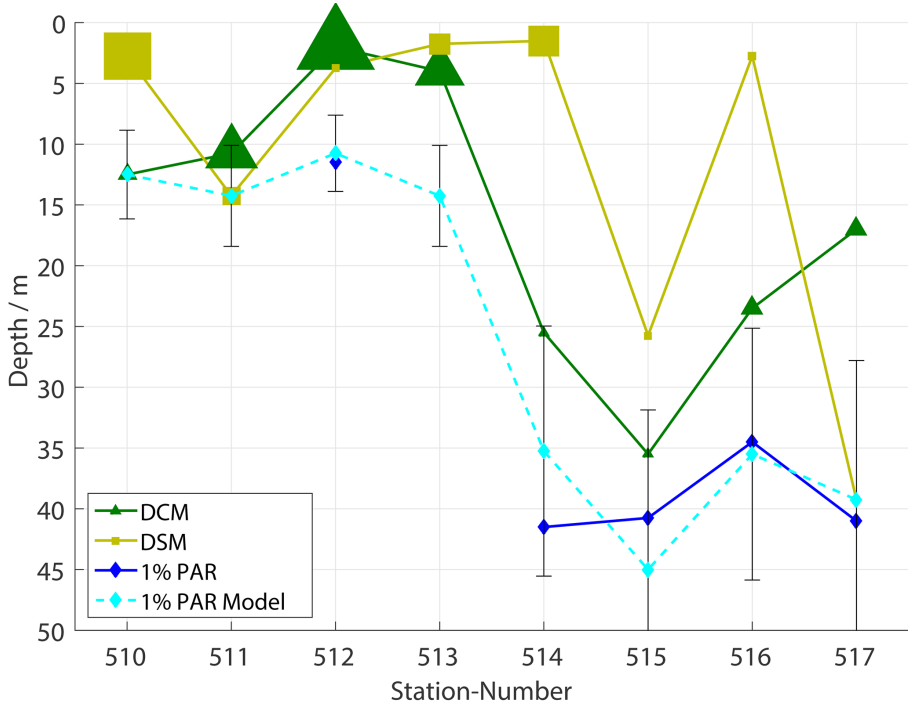

Figure 9. DCM (green, deep chlorophyll max) and DSM (ocher, deep SPMi max) at stations in the Vaigat (510–513) and Disko Bay (514–517). The size of the markers represents the sum of Chl and SPMi concentrations from the top of the water column to the modeled 1 % depth. Measured 1 % PAR (blue) where available and modeled 1 % PAR as dashed line (cyan).

OSD
12, 1537–1566, 2015